Research Article

Merfat H. Raddadi, Shreen El-Sapa, Mahjoub A. Elamin, Houda Chtioui, Riadh Chteoui, Alaa A. El-Bary, and Khaled Lotfy*

Optoelectronic–thermomagnetic effect of a microelongated non-local rotating semiconductor heated by pulsed laser with varying thermal conductivity

https://doi.org/10.1515/phys-2023-0145
received August 25, 2023; accepted November 03, 2023

Abstract: In this study, we investigated the effect of a rotation field and magnetic field on a homogeneous photo-thermoelastic nonlocal material and how its thermal conductivity changes as a result of a linearly distributed thermal load. The thermal conductivity of an interior particle is supposed to increase linearly with temperature under the impact of laser pulses. Microelastic (microelements distribution), non-local semiconductors are used to model the problem under optoelectronic procedures, as proposed by the thermoelasticity theory. According to the microelement transport processes, the micropolar-photothermoelasticity theory accounts for the medium's microelongation properties. This mathematical model is solved in two dimensions using the harmonic wave analysis. Nonlocal semiconductor surfaces can generate completely dimensionless displacement, temperature, microelongation, carrier density, and stress components with the appropriate boundary conditions. The effects of thermal conductivity, thermal relaxation times, magnetic pressure effect, laser pulses, and rotation parameters on wave propagation in silicon (Si) material are investigated and graphically displayed for a range of values.

Keywords: magnetic field, micro-elongation, optoelectronic, laser pulsed, rotation field, thermal conductivity

*** Corresponding author: Khaled Lotfy,** Department of Mathematics, Faculty of Science, Zagazig University, P.O. Box 44519, Zagazig, Egypt; Department of Mathematics, College of Science, Taibah University, P.O. Box 344, Al-Madinah Al-Munawarah, 30002, Saudi Arabia, e-mail: khlotf_1y@yahoo.com
Merfat H. Raddadi: Department of Mathematics, College of Science, Taibah University, P.O. Box 344, Al-Madinah Al-Munawarah, 30002, Saudi Arabia, e-mail: Mhraddadi@taibshu.edu.sa
Shreen El-Sapa: Department of Mathematical Sciences, College of Science, Princess Nourah bint Abdulrahman University, P.O. Box 84428, Riyadh 11671, Saudi Arabia, e-mail: seelsapa@pnu.edu.sa
Mahjoub A. Elamin: Department of Mathematics, University College of Umluj, University of Tabuk, Umluj, Saudi Arabia, e-mail: Malshaygi@ut.edu.sa
Houda Chtioui: Department of Physics, Faculty of Sciences, University of Monastir, Monastir, Tunisia, e-mail: chtiouihouda1974@yahoo.com
Riadh Chteoui: Department of Basic Sciences, University of Tabuk, Duba, Tabuk, Saudi Arabia, e-mail: ralshtaiwi@ut.edu.sa
Alaa A. El-Bary: Arab Academy for Science, Technology and Maritime Transport, P.O. Box 1029, Alexandria, Egypt, e-mail: aaelbary@aast.edu

Nomenclature

$\lambda,\ \mu$	elastic parameters
$\delta_n = (3\lambda + 2\mu)d_n$	potential difference
T_0	reference temperature
$\hat{\gamma} = (3\lambda + 2\mu)\alpha_{t_1}$	volume thermal expansion
σ_{ij}	microelongational stress tensor
ρ	medium density
α_{t_1}	thermal expansion coefficient
$e = \frac{\partial u}{\partial x} + \frac{\partial w}{\partial z}$	dilatation in 2D
C_e	specific heat of the microelongated material
K	thermal conductivity
D_E	carrier diffusion
τ	lifetime
E_g	energy gap
e_{ij}	strain tensor
Π, Ψ	two scalar functions
j_0	microinertia of microelement
$a_0,\ \alpha_0, \lambda_0, \lambda_1$	microelongational material parameters
τ_0, ν_0	thermal relaxation times
φ	scalar microelongational function
m_k	microstretch vector
$s = s_{kk}$	stress tensor component
δ_{ik}	Kronecker delta

$\underline{n}$	unit vector in the direction of the y-axis
$\underline{\Omega} = \Omega\underline{n}$	angular velocity
ξ	length-related elastic nonlocal parameter
l	external characteristic length scale
a	internal characteristic length
e_0	non-dimensional material property
α_{t_2}	linear micro-elongation coefficient

1 Introduction

Nanostructured semiconductors are now under development in the semiconductor industry, and their behavior has become a major focus of research in recent years. The physical, electrical, and optical characteristics of nanostructures are profoundly affected by the interplay between property and structure. Nanostructures, which have dimensions on the nanometer scale, have unique properties due to their small size and large surface area. Thermodynamic and elastic mechanisms within these materials have been better understood because of the investigation of nanostructures. Researchers have developed models to explore the impact of nano-dimension and structural properties on the behavior of nano-structures, and these models have been tested using both experimental techniques and computer simulations. Since scientists now have a better grasp on how nanostructures function, exciting new technology possibilities have opened up. Electronics, optoelectronics, catalysis, energy storage, sensors, and biomedical devices are just some of the many applications that have benefited from nanostructured materials. They are of great interest in the creation of high-tech materials with improved performance and usefulness because of their outstanding qualities. Traditional continuum mechanics, which treat matter as continuous, can only describe solids' macroscopic mechanical behavior because microelements determine microstructure. Continuity mechanics must consistently account for microinertia since macroscopic and microscopic scales are relevant. In conclusion, semiconductors must be elastic to be considered thermoelastic. Due to the link between thermoelastic and electronic deformation (TED and ED). The ED uses semiconductor crystal lattice photo-generation theory. Semiconductors microelongate because their internal resistance decreases with temperature. Given this, investigating how light thermal energy influences material microelongation and microinertia is critical. This discovery underpins the photothermal (PT) theory, which states that surfaces stimulate free electrons during transition phases.

The traditional deformation medium hypothesis of microelongation classifies micro-elongated media as follows: gaseous or non-viscous fluid pores, solid–liquid crystals, and elastic fiber composites. This suggests that microscopic material particles undergo volumetric elongation. Material sites in the deformation medium shrink and stretch independently. The semiconductor's internal structure changes due to light's thermal influence and microelongation parameters. Microelongation requires thermal deformation, but micropolar deformation requires electron rotation [1]. This study analyzed semiconductor materials using microstretch and micropolar theories. Microstretch theory becomes microelongational for electrons with orthogonal and contracting degrees of freedom. Eringen [2,3] introduced a micropolar theory-based microstretch-thermoelasticity model to account for solid medium microstructure. Microstretch thermoelasticity is used to examine elastic substances in many applications [4–6]. Abouelregal and Marin [7,8] investigated the nanobeam responses of a dipolar elastic body with temperature-dependent properties. Numerous hydrodynamic applications of microstretch theory are used to explore Casson fluid flow in porous media [9,10]. In contrast, Ezzat and Abd-Elaal [11] examined the flow layer in a viscoelastic porous medium with a single relaxation time under various viscoelastic conditions. Microelongated elastic media are studied, and wave propagation is calculated using internal heat source impact [12,13]. Ailawalia *et al.* [14–16] investigated the impact of an internal heat source on plane strain deformation by acquiring knowledge of microelongated elastic material equations. Micropolar theory of the elastic body is demonstrated in the two-phase porosity medium [17,18].

The photoacoustic and photothermal (PT) theory has been widely adopted in recent years for studies of semiconductor materials [19,20]. Numerous authors [21,22] examined how to effectively personify photoacoustic and PT technologies through the use of metaphors and similes. We can investigate the interplay between PT and thermoelasticity theories by deforming semiconductor material in two dimensions [23]. According to ED, microcantilever technologies are used to investigate the optical characteristics of semiconductors [24,25]. Different researchers have developed models that can be used to represent the interplay of mechanical, optical, thermal, and elastic waves following the photo-thermoelasticity theory of elastic semiconductor media [26–28]. A photo-thermoelastic excitation model in the two-temperature theory was investigated. This model takes into account the dynamic thermal conductivity of elastic semiconductor media. Abbas *et al.* [29] employed the dual-phase delay model with PT interaction. The PT transport processes in a semiconductor medium were analyzed by Mahdy *et al.* [30] using the microstretch theory while the medium was

rotated. However, the photo-microstretch theory for a semiconductor elastic media was investigated by Lotfy and El-Bary [31] using electro-magneto-thermoelasticity.

Eringen and Edelen [32] developed the nonlocal elasticity hypothesis by applying the principles of global balancing rules and the second law of thermodynamics in their work. The theory of nonlocal elasticity [33] initially focused on screw dislocations and surface waves in solids as its primary areas of investigation. Chteoui *et al.* [34] conducted research to study the effect that Hall current has on nonlocality semiconductor medium to get optical, elastic, thermal, and diffusive waves. However, Sheoran *et al.* [35,36] studied the nonlocality material using the thermodynamical vibrations under the effect of magnetic field with temperature-dependent properties. On the other hand, Chaudhary *et al.* [37] investigated the PT interactions of fiber-reinforced semiconductor material under a dual-phase-lag model. Biswas [38–40] studied many problems to obtain the behavior of surface wave propagation in non-local thermoelastic porous media. Tiwari *et al.* [41–43] used the memory-dependent derivatives to study non-local photo-thermoelastic media according to variable thermal properties using the dual-phase-lag model and sinusoidal heat source. Singhal *et al.* [44] introduced a comparative study to obtain the effect of piezoelectric and flexoelectric effects on wave vibration of different thermoplastic materials. Nirwal *et al.* [45] used the piezo-composite medium to study the secular equation of SH waves with flexoelectric. Sahu *et al.* [46] studied the surface wave propagation of magneto-electro-elastic media with functionally graded properties. On the other hand, Kaur and Singh [47,48] investigated the memory-dependent derivative and fractional order heat to obtain the wave propagation of a nonlocality semiconductor medium in the context of photo-thermoelasticity theory with forced transverse vibrations. The functionally graded properties and Hall effect of nonlocal thermoelastic semiconductor according to the Moore–Gibson–Thompson photo-thermoelastic mode are studied [49]. Sarkar *et al.* [50,51] used the dual-phase-lag thermoelastic models to study the wave propagation of non-local vibrations semiconducting elastic void medium according to the functionally graded properties. Sharma *et al.* [52] investigated the vibrations of a nonlocal thermoelastic with heat exchanger to obtain the thermal performance. The theory of thermoelasticity according to the modified models with vibration analysis of functionally graded properties is used to investigate the nonlocal effect on thermoelastic materials [53].

This study investigated the TED and TE deformation in a microelongated (microelements) stimulated medium. This study investigated the effects of non-locality, rotational field, altered thermal conductivity, and photo-thermomechanical phenomena under the influence of laser pulses and magnetic field. By selecting the basic physical fields in a dimensionless manner, the governing equations can be expressed with the two-dimensional deformation of the space. Normal-mode analysis is performed to obtain thorough analytical solutions for the main variables being studied, taking into account specific conditions at the boundary of the nonlocal medium. Several graphics are employed to compare the waves propagated by the physical field variables in four different settings. The contexts encompass the impact of laser pulses, rotational factors, the effects of thermal memory, magnetic field, and the variation in thermal conductivity.

2 Theoretical model and basic equations

The dynamics of electric and magnetic fields, as well as their interactions, are governed by Maxwell's equations. The development of charge and current, their genesis and expansion, and their mutual impacts are all described by the equations. In the presence of a main magnetic field $\vec{H}$, the presence of an induced electric field $\vec{E}$ and a magnetic field $\vec{h}$ will be shown by the basic equations. These equations (without the charge density) express the simplified form of Maxwell's equations, which describe the electromagnetic field in the electrodynamics of an elastic and evenly conductive material under ideal temperature and electrical conditions, given as [13,14]:

$$\left.\begin{aligned} &\vec{J} = \operatorname{curl}\vec{h} - \varepsilon_0\frac{\partial\vec{E}}{\partial t}, \quad \operatorname{curl}\vec{E} = -\mu_0\frac{\partial\vec{H}}{\partial t}, \\ &\vec{E} = -\mu_0\left(\frac{\partial\vec{u}}{\partial t}\times\vec{H}\right), \quad \operatorname{div}\vec{H} = 0,\ \vec{h} = H_0(0,\ e,\ 0), \end{aligned}\right\}. \tag{1}$$

where $\vec{J}$ is the current density, μ_0 is the magnetic permeability, and ε_0 is the electric permeability. In this case, the Lorentz's force $\vec{F}$ of electromagnetic field can be obtained as:

$$\left.\begin{aligned} &E_x = \mu_0 H_0\dot{w},\ E_y = 0,\ E_z = -\mu_0 H_0\dot{u},\ \vec{H} = (0, H_0, 0), \\ &J_x = -\left(\frac{\partial h}{\partial z} + \mu_0 H_0\varepsilon_0\ddot{w}\right),\ J_y = 0,\ J_z = \frac{\partial h}{\partial x} + \mu_0 H_0\varepsilon_0\ddot{u}, \\ &\vec{F} = \mu_0(\vec{J}\times\vec{H}) = \left(-\mu_0 H_0\frac{\partial e}{\partial x} - \varepsilon_0\mu_0^2 H_0^2\frac{\partial^2 u}{\partial t^2},\ 0,\ -\mu_0 H_0\frac{\partial e}{\partial z}\right. \\ &\qquad \left. - \varepsilon_0\mu_0^2 H_0^2\frac{\partial^2 w}{\partial t^2}\right). \end{aligned}\right\}. \tag{2}$$

There are four fundamental quantities introduced in this problem, all of which are presented in Cartesian coordinates (Figure 1): carrier density N (photo-electronic

according to the plasma wave propagation), the gradient temperature T (thermal distribution), elastic waves u_i (displacement), and the scalar microelongational function φ. Under the action of a uniform rotating field ($\underline{\Omega} = \Omega \underline{n}$), directed with unitary $\underline{n}$ on the y-axis, the fundamental equations of a non-local semiconductor medium are provided in a rounded two-dimensional (2D) form. For a body-force-free semiconductor medium, the rotationally varying thermal conductivity field equations and constitutive relations under the impact of magnetic field are as follows [54,55]:

I) Non-local photo-thermoelastic microelongated constitutive equations are as follows [12,24]:

$$\left.\begin{aligned}
&\sigma'_{iI} = (\lambda_0\varphi + \lambda u_{r,r})\delta_{iI} + 2\mu u_{I,i} - \hat{\gamma}\left(1 + v_0\frac{\partial}{\partial t}\right)T\delta_{iI} \\
&\qquad - ((3\lambda + 2\mu)d_n N)\delta_{iI}, \\
&m_i = a_0\varphi_{,i}, \quad (1 - \xi^2\nabla^2)\sigma_{iI} = \sigma'_{iI}, \\
&s - (1 - \xi^2\nabla^2)\sigma' = \lambda_0 u_{i,i} - \hat{\gamma}\left(1 + v_0\frac{\partial}{\partial t}\right)T - ((3\lambda \\
&\qquad + 2\mu)d_n N)\delta_{2i} + \lambda_1\varphi, \\
&\xi = \frac{ae_0}{l}.
\end{aligned}\right\} \quad (3)$$

II) The equation for waves in a connected plasma (2) can be written as [23]:

$$\dot{N} = D_E N_{,ii} - \frac{N}{\tau} + \kappa\frac{T}{\tau}. \quad (4)$$

III) The processes involving microelements determine the equation of motion and the microelongation equation for non-local medium under the effect of the magnetic field, which can be written as [56]:

$$\left.\begin{aligned}
&(\lambda + \mu)u_{j,ij} + \mu u_{i,jj} + \lambda_o\varphi_{,i} - \hat{\gamma}\left(1 + v_0\frac{\partial}{\partial t}\right)T_{,i} - \delta_n N_{,i} \\
&\quad + F_i = \rho((1 - \xi^2\nabla^2)\ddot{u}_i + \{\vec{\Omega}x(\vec{\Omega}x\vec{u})\}_i \\
&\quad + (2\underline{\vec{\Omega}}x\dot{\vec{u}})_i)
\end{aligned}\right\} \quad (5)$$

$$a_0\varphi_{,ii} - \lambda_1\varphi - \lambda_0 u_{j,j} + \hat{\gamma}_1\left(1 + v_0\frac{\partial}{\partial t}\right)T = \frac{1}{2}j_0\rho\ddot{\varphi}. \quad (6)$$

IV) The non-local model of the heat equation can be expressed without the presence of a heat source as [16]:

$$(KT_{,i})_{,i} - \rho C_E\left(n_1 + \tau_0\frac{\partial}{\partial t}\right)\dot{T} - \hat{\gamma}T_0\left(n_1 + n_0\tau_0\frac{\partial}{\partial t}\right)\dot{u}_{i,i} + \frac{E_g}{\tau}N = \hat{\gamma}_1 T_0\dot{\varphi}, \quad (7)$$

where $\dot{\square} = \frac{\partial \square}{\partial t}$, $\hat{\gamma}_1 = (3\lambda + 2\mu)\alpha_{t_2}$, $\kappa = \frac{\partial n_0}{\partial T}\frac{T}{\tau}$, and $\square_{,i} = \frac{\partial \square}{\partial x_i}$.

Temperature affects thermal conductivity in a non-local microelongated semiconductor material. Thermal conductivity is proportional to temperature, as shown by a linear function. In this situation, light beams' thermal influence simplifies thermal conductivity [57]:

$$K = K_0(1 + \pi T), \quad (8)$$

where $\pi \le 0$ is a negligible constant. The reference thermal conductivity for a temperature-independent medium is the physical constant K_0. The nonlinear components in thermal conductivity can be transformed into linear ones using the integral form of Kirchhoff's transform theory of temperature [57]:

$$\Theta = \frac{1}{K_0}\int_0^T K(\Re)\mathrm{d}\Re. \quad (9)$$

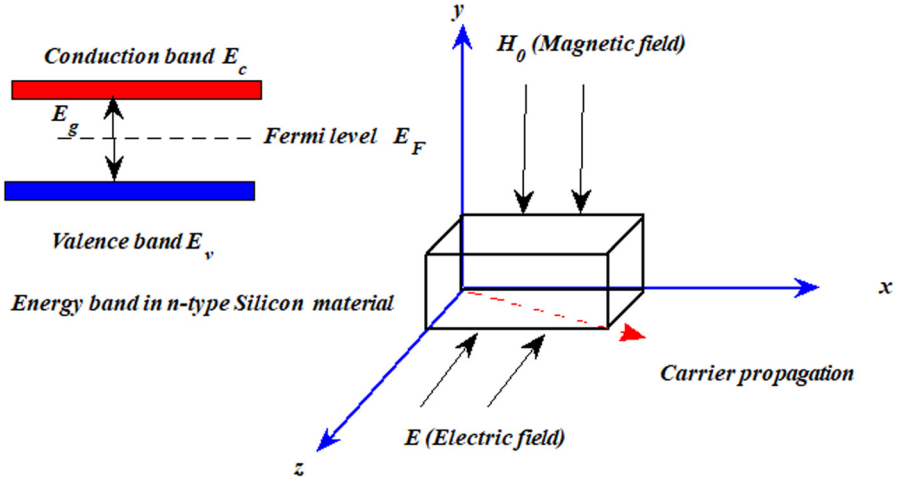

Figure 1: Geometry of the problem.

It is possible to express the 2D deformation in terms of the following quantities in space (xz-plane) and time coordinates (t) as: $\vec{u} = (u, 0, w)(x, z, t)$; $\varphi = \varphi(x, z, t)$.

Two-dimensional (2D) basic Eqs. (4)–(6) can be simplified as:

$$\left.\begin{aligned}(\lambda+\mu)\left(\frac{\partial^2 u}{\partial x^2}+\frac{\partial^2 w}{\partial x\partial z}\right)+\mu\left(\frac{\partial^2 u}{\partial x^2}+\frac{\partial^2 u}{\partial z^2}\right)\\ +\lambda_0\frac{\partial\varphi}{\partial x}-\hat{\gamma}\left(1+v_0\frac{\partial}{\partial t}\right)\frac{\partial T}{\partial x}-\delta_n\frac{\partial N}{\partial x}\\ =\rho\left((1-\xi^2\nabla^2)\frac{\partial^2 u}{\partial t^2}-\Omega^2 u+2\Omega\frac{\partial w}{\partial t}\right)\end{aligned}\right\}, \tag{10}$$

$$\left.\begin{aligned}(\lambda+\mu)\left(\frac{\partial^2 u}{\partial x\partial z}+\frac{\partial^2 w}{\partial z^2}\right)+\mu\left(\frac{\partial^2 w}{\partial x^2}+\frac{\partial^2 w}{\partial z^2}\right)\\ +\lambda_0\frac{\partial\varphi}{\partial z}-\hat{\gamma}\left(1+v_0\frac{\partial}{\partial t}\right)\frac{\partial T}{\partial z}-\delta_n\frac{\partial N}{\partial z}\\ =\rho\left((1-\xi^2\nabla^2)\frac{\partial^2 w}{\partial t^2}-\Omega^2 w-2\Omega\frac{\partial u}{\partial t}\right)\end{aligned}\right\}, \tag{11}$$

$$\begin{aligned}a_0\left(\frac{\partial^2\varphi}{\partial x^2}+\frac{\partial^2\varphi}{\partial z^2}\right)-\lambda_1\varphi-\lambda_0 e+\hat{\gamma}_1\left(1+v_0\frac{\partial}{\partial t}\right)T\\ =\frac{1}{2}j\rho\frac{\partial^2\varphi}{\partial t^2}.\end{aligned} \tag{12}$$

Different photo-thermoelasticity models (coupled-dynamical, $n_1 = 1$, $n_0 = \tau_0 = v_0 = 0$, Lord and Shulman [$n_1 = n_0 = 1, v_0 = 0, \tau_0 > 0$], and Green and Lindsay [GL, $n_1 = 1$, $n_0 = 0$, $v_0 \geq \tau_0 > 0$] are governed by the specified parameters n_1 and n_0 at the thermal relaxation durations v_0 and τ_0 [58–60]. Incorporating the thermal conductivity variable into computations can be done by using Eqs. (8) and (9), as shown by the following differentiation relations:

$$\left.\begin{aligned}&K_0\Theta_{,i}=K(T)T_{,i},\ K_0\frac{\partial\theta}{\partial t}=K(T)\frac{\partial T}{\partial t},\ \frac{K_0}{K(T)}\Theta_{,i}=T_{,i},\\ &K_0\Theta_{,ii}=(K(T)T_{,i})_{,i}\end{aligned}\right\}. \tag{13}$$

The effects of the map transformation and differentiation allow us to rewrite Eq. (4) as:

$$\left.\begin{aligned}\frac{\partial}{\partial t}\frac{\partial N}{\partial x_j}&=D_{\mathrm{E}}\frac{\partial N_{,ii}}{\partial x_j}-\frac{1}{\tau}\frac{\partial N}{\partial x_j}+\frac{\kappa}{\tau}\frac{\partial T}{\partial x_j},\\ \frac{\partial}{\partial t}\frac{\partial N}{\partial x_j}&=D_{\mathrm{E}}\frac{\partial N_{,ii}}{\partial x_j}-\frac{1}{\tau}\frac{\partial N}{\partial x_j}+\frac{\kappa K_0}{\tau K}\frac{\partial\Theta}{\partial x_j},\\ \frac{\partial}{\partial t}\frac{\partial N}{\partial x_j}&=D_{\mathrm{E}}\frac{\partial N_{,ii}}{\partial x_j}-\frac{1}{\tau}\frac{\partial N}{\partial x_j}+\frac{\kappa}{\tau}\frac{\partial\Theta}{\partial x_j}\end{aligned}\right\}, \tag{14}$$

The non-linear variables were disregarded when solving for the missing piece of the previous Eq. (13) using the Taylor expansion:

$$\left.\begin{aligned}\frac{\kappa K_0}{\tau K}\frac{\partial\Theta}{\partial x_j}&=\frac{\kappa K_0}{K_0\tau(1+\pi T)}\frac{\partial\Theta}{\partial x_j}=\frac{\kappa}{\tau}(1+\pi T)^{-1}\frac{\partial\Theta}{\partial x_j}\\ &=\frac{\kappa}{\tau}(1-\pi T+(\pi T)^2-\ldots)\frac{\partial\Theta}{\partial x_j}=\\ \frac{\kappa}{\tau}\frac{\partial\Theta}{\partial x_j}-\frac{\kappa}{\tau}\pi T\frac{\partial\Theta}{\partial x_j}+\frac{\kappa}{\tau}(\pi T)^2\frac{\partial\Theta}{\partial x_j}-\ldots&=\frac{\kappa}{\tau}\frac{\partial\Theta}{\partial x_j}\end{aligned}\right\}. \tag{15}$$

By applying Eq. (15) to the result of integrating Eq. (14), we obtain the following:

$$\frac{\partial N}{\partial t}=D_{\mathrm{E}}N_{,ii}-\frac{1}{\tau}N+\frac{\kappa}{\tau}\Theta. \tag{16}$$

In this scenario, the map transform (9) can be used to simplify the non-local microelongated heat Eq. (7) as follows:

$$\begin{aligned}\Theta_{,ii}-\frac{1}{k}\left(n_1+\tau_0\frac{\partial}{\partial t}\right)\frac{\partial\Theta}{\partial t}-\frac{\hat{\gamma}T_0}{K_0}\left(n_1+n_0\tau_0\frac{\partial}{\partial t}\right)\dot{u}_{i,i}+\frac{E_{\mathrm{g}}}{K_0\tau}N\\ =\frac{\hat{\gamma}_1T_0}{K_0}\dot{\varphi},\end{aligned} \tag{17}$$

where the thermal diffusivity of the nonlocality medium is $\frac{1}{k}=\frac{\rho C_{\mathrm{E}}}{K_0}$.

The following non-dimensional quantities provided help make broad strokes with the numerical simulations:

$$\left.\begin{aligned}&\bar{N}=\frac{\delta_n}{2\mu+\lambda}N,\quad(\bar{x}_i,\ \bar{\xi},\ \bar{u}_i)=\frac{1}{\omega^* C_{\mathrm{T}}}(x_i,\ \xi, u_i),\\ &(\bar{t},\ \bar{\tau}_0,\ \bar{v}_0)=\frac{(t,\ \tau_0, v_0)}{\omega^*},\\ &C_{\mathrm{T}}^2=\frac{2\mu+\lambda}{\rho},\quad\bar{\Theta}=\frac{\hat{\gamma}\Theta}{2\mu+\lambda},\quad\bar{\sigma}_{ij}=\frac{\sigma_{ij}}{2\mu+\lambda},\\ &\bar{\varphi}=\frac{\rho C_T^2}{T_0\hat{\gamma}}\varphi,\quad\omega^*=\frac{K_0}{\rho C_{\mathrm{E}}C_{\mathrm{T}}^2},\\ &(\bar{\Pi},\bar{\psi})=\frac{(\Pi,\psi)}{(C_{\mathrm{T}}\omega^*)^2},C_L^2=\frac{\mu}{\rho},\ \bar{\Omega}=\omega^*\Omega.\end{aligned}\right\} \tag{18}$$

With the dimensionless Eq. (18) (without the superscripts), the fundamental equations can be rearranged as follows:

$$\left(\nabla^2-\varepsilon_3-\varepsilon_2\frac{\partial}{\partial t}\right)N+\varepsilon_4\Theta=0, \tag{19}$$

$$\left.\begin{aligned}&(1-\xi^2\nabla^2+\varepsilon_0\mu_0^2H_0^2)\frac{\partial^2 u}{\partial t^2}-\Omega^2u+2\Omega\frac{\partial w}{\partial t}\\ &=\frac{1}{\rho C_{\mathrm{T}}^2}((\lambda+\mu)-\mu_0H_0^2)\frac{\partial e}{\partial x}\\ &+\frac{\mu}{\rho C_T^2}\nabla^2u+\frac{T_0\hat{\gamma}\lambda_0}{(\rho C_{\mathrm{T}}^2)^2}\frac{\partial\varphi}{\partial x}-\left(1+v_0\frac{\partial}{\partial t}\right)\frac{\partial\Theta}{\partial x}-\frac{\partial N}{\partial x}\end{aligned}\right\}, \tag{20}$$

$$\left.\begin{aligned}&(1-\xi^2\nabla^2+\varepsilon_0\mu_0^2H_0^2)\frac{\partial^2 w}{\partial t^2}-\Omega^2 w-2\Omega\frac{\partial u}{\partial t}\\&=\frac{1}{\rho C_{\mathrm{T}}^2}((\lambda+\mu)-\mu_0H_0^2)\frac{\partial e}{\partial z}\\&+\frac{\mu}{\rho C_{\mathrm{T}}^2}\nabla^2 w+\frac{T_0\hat{\gamma}\lambda_0}{(\rho C_T^2)^2}\frac{\partial\varphi}{\partial z}-\left(1+v_0\frac{\partial}{\partial t}\right)\frac{\partial\Theta}{\partial z}-\frac{\partial N}{\partial z}\end{aligned}\right\},\quad(21)$$

$$\left(\nabla^2-C_3-C_4\frac{\partial^2}{\partial t^2}\right)\varphi-C_5e+C_6\left(1+v_0\frac{\partial}{\partial t}\right)\Theta=0,\quad(22)$$

$$\begin{aligned}&\nabla^2\Theta-\left(n_1+\tau_0\frac{\partial}{\partial t}\right)\frac{\partial\Theta}{\partial t}-\varepsilon\left(n_1+n_0\tau_0\frac{\partial}{\partial t}\right)\frac{\partial e}{\partial t}+\varepsilon_5N\\&=\varepsilon_1\frac{\partial\varphi}{\partial t}.\end{aligned}\quad(23)$$

The displacement components can be introduced in terms of the potential scalar $\Pi(x,z,t)$ and the vector space-time $\Psi(x,z,t)$ functions as: $\vec{u}$ = grad Π + curl Ψ. In this case, the system of Eqs. (20)–(23) can be expressed as:

$$\begin{aligned}&\left(\left(\alpha+\xi^2\frac{\partial^2}{\partial t^2}\right)\nabla^2+\Omega^2-\mathbb{R}_{\mathrm{H}}\frac{\partial^2}{\partial t^2}\right)\Pi+2\Omega\frac{\partial\psi}{\partial t}\\&+\left(1+v_o\frac{\partial}{\partial t}\right)\Theta+a_1\varphi-N=0,\end{aligned}\quad(24)$$

$$\left(\left(1+\xi^2\frac{\partial^2}{\partial t^2}\right)\nabla^2-a_3\Omega^2-a_3\mathbb{R}_{\mathrm{H}}\frac{\partial^2}{\partial t^2}\right)\psi-a_3^*\frac{\partial\Pi}{\partial t}=0,\quad(25)$$

$$\left(\nabla^2-C_3-C_4\frac{\partial^2}{\partial t^2}\right)\varphi-C_5\nabla^2\Pi+C_6\left(1+v_0\frac{\partial}{\partial t}\right)\Theta=0,\quad(26)$$

$$\begin{aligned}&\left(\nabla^2-\left(n_1\frac{\partial}{\partial t}+\tau_0\frac{\partial^2}{\partial t^2}\right)\right)\Theta-\varepsilon\left(n_1\frac{\partial}{\partial t}+n_o\tau_0\frac{\partial^2}{\partial t^2}\right)\nabla^2\Pi+\varepsilon_5N\\&-\varepsilon_1\frac{\partial\varphi}{\partial t}=0.\end{aligned}\quad(27)$$

It is possible to rewrite the constitutive relations in 2D and dimensionless as [24]:

$$\left.\begin{aligned}(1-\xi^2\nabla^2)\sigma_{xx}&=\frac{\partial u}{\partial x}+a_2\frac{\partial w}{\partial z}-\left(1+v_0\frac{\partial}{\partial t}\right)\Theta-N+a_1\varphi,\\(1-\xi^2\nabla^2)\sigma_{zz}&=a_2\frac{\partial u}{\partial x}+\frac{\partial w}{\partial z}-\left(1+v_0\frac{\partial}{\partial t}\right)\Theta-N+a_1\varphi,\\(1-\xi^2\nabla^2)\sigma_{xz}&=a_4\left(\frac{\partial u}{\partial z}+\frac{\partial w}{\partial x}\right),\end{aligned}\right\}.\quad(28)$$

where

$$\begin{aligned}a_1&=\frac{T_0\hat{\gamma}\lambda_0}{(\rho C_{\mathrm{T}}^2)^2},\ a_2=\frac{\lambda}{\rho C_{\mathrm{T}}^2},\ a_3=\frac{\rho C_{\mathrm{T}}^2}{\mu},\ \varepsilon=\frac{\hat{\gamma}^2\omega^*T_0}{K_0\rho},\\&\varepsilon_1=\frac{\hat{\gamma}_1\hat{\gamma}^2\omega^*T_0}{K_0\rho(2\mu+\lambda)},\varepsilon_2=\frac{\omega^*C_{\mathrm{T}}^2}{D_{\mathrm{E}}},a_3{}^*=2\Omega a_3,\\a_4&=\frac{\mu}{\rho C_{\mathrm{T}}^2},\ C_4=\frac{\rho jC_{\mathrm{T}}^2}{2\alpha_0},\ \varepsilon_3=\frac{\omega^{*2}C_{\mathrm{T}}^2}{\tau D_{\mathrm{E}}},\varepsilon_4=\frac{\kappa d_n\omega^{*2}\rho}{\tau D_{\mathrm{E}}\alpha_{\mathrm{t1}}},\\&\varepsilon_5=\frac{E_g\hat{\gamma}\omega^{*2}C_{\mathrm{T}}^2}{\tau K_0\delta_n},C_3=\frac{\lambda_1C_{\mathrm{T}}^2\omega^{*2}}{\alpha_0},\ C_5=\frac{\lambda_0\rho C_{\mathrm{T}}^4\omega^{*2}}{\alpha_0T_0\hat{\gamma}},\\C_6&=\frac{\hat{\gamma}_1\rho\omega^{*2}T_0}{\hat{\gamma}\alpha_0},\ \mathbb{R}_{\mathrm{H}}=1+\varepsilon_0\mu_0^2H_0^2/\rho,\ \ \alpha=1+\frac{\mu_0H_0^2}{\rho\omega^*C_{\mathrm{T}}}.\end{aligned}$$

3 Normal-mode technique

The following formula can be used to express the solutions for the considered physical variables $M(x,\ z,\ t)$ in terms of normal modes [39]:

$$M(x,\ z,\ t)=\bar{M}(x)e^{ibz}e^{\omega t}.\quad(29)$$

The value of $\bar{M}$ represents the amplitude of M with the wave number in the z-direction b and $i=\sqrt{-1}$. The complex frequency denotes $\omega=\omega_0+i\zeta$, where ω_0 and ζ are the arbitrary factors. The basic Eqs. (19) and (24–27) are rewritten as follows using Eq. (29):

$$(D^2-a_1)\bar{N}+\varepsilon_4\bar{\Theta}=0,\quad(30)$$

$$(D^2-A_1)\bar{\Pi}+A_9\bar{\psi}+A_2\bar{\Theta}+a_1^*\bar{\varphi}-a_2^*\bar{N}=0,\quad(31)$$

$$(D^2-A_3)\bar{\psi}-A_{10}\bar{\Pi}=0,\quad(32)$$

$$(D^2-A_4)\bar{\varphi}-C_5(D^2-b^2)\bar{\Pi}+A_5\bar{\Theta}=0,\quad(33)$$

$$(D^2-A_6)\bar{\Theta}-A_7(D^2-b^2)\bar{\Pi}+\varepsilon_5\bar{N}-A_8\bar{\varphi}=0,\quad(34)$$

$$\left.\begin{aligned}(1-\xi^2(D^2-b^2))\bar{\sigma}_{xx}&=D\bar{u}+iba_2\bar{w}-A_2\bar{\Theta}-\bar{N}+a_1\bar{\varphi},\\(1-\xi^2(D^2-b^2))\bar{\sigma}_{zz}&=a_2D\bar{u}+ib\bar{w}-A_2\bar{\Theta}-\bar{N}+a_1\bar{\varphi},\\(1-\xi^2(D^2-b^2))\sigma_{xz}&=a_4(ib\bar{u}+D\bar{w}).\end{aligned}\right\}.\quad(35)$$

where

$$\left.\begin{aligned} &a_1 = b^2 + \varepsilon_3 + \varepsilon_2\omega, A_1 = ab^2 + \frac{\mathbb{R}_H\omega^2}{\alpha + \xi^2\omega^2} - \Omega^2,\\ &A_3 = b^2 + \frac{a_3(\Omega^2 + \mathbb{R}_H\omega^2)}{1 + \xi^2\omega^2}, A_{10} = \frac{a_3^*\omega}{1 + \xi^2\omega^2},\\ &D = \frac{\mathrm{d}}{\mathrm{d}x}, A_4 = b^2 + C_3 + C_4\omega^2, A_5 = C_6(1 + \nu_0\omega),\\ &A_2 = \frac{1 + \nu_o\omega}{\alpha + \xi^2\omega^2}, a_2^* = \frac{1}{\alpha + \xi^2\omega^2},\\ &A_6 = b^2 + (n_1\omega + n_0\tau_0\omega^2), A_7 = \varepsilon(n_1\omega + n_o\tau_o\omega^2),\\ &A_8 = \varepsilon_1\omega, A_9 = \frac{2\Omega\omega}{\alpha + \xi^2\omega^2}, a_1^* = \frac{a_1}{\alpha + \xi^2\omega^2}. \end{aligned}\right\} \quad (36)$$

The solution to the system of Eqs. (30)–(34) is obtained as follows:

$$\{D^{10} - B_1D^8 + B_2D^6 - B_3D^4 + B_4D^2 - B_5\}(\bar{\varphi}, \bar{N}, \bar{\Theta}, \bar{\Pi}, \bar{\psi}) = 0, \quad (37)$$

where

$$B_1 = -\{A_2A_7 + C_5a_1^* - A_1 - A_3 - A_4 - a_2^*A_6 - \alpha_1\},$$

$$B_2 = \left\{\begin{aligned} &(-A_2A_7 - C_5a_1^* + A_1 + A_3 + A_4 + A_6)\alpha_1 + ((-b^2 - A_3\\ &\quad - A_6)C_5 - A_5A_7)a_1^* + A_2A_8C_4 + A_5A_8 +\\ &(-b^2A_2 - A_2A_3 - A_2A_4 + \varepsilon_4)A_7 + (A_1 + A_3 + A_4)A_6\\ &\quad + a_2^*(A_1 + A_3)A_4 + A_1A_3 + A_9A_{10} - \varepsilon_4\varepsilon_5 \end{aligned}\right\},$$

$$B_3 = -\left\{\begin{aligned} &(-C_5a_1^* + A_1 + A_3 + A_4)\varepsilon_4\varepsilon_5 + (A_7(-b^2 - A_3\\ &\quad - A_4) + A_8C_5)\varepsilon_4 + (-A_2A_3A_8 + A_3A_6a_1^* +\\ &(-A_3A_4 - A_6(A_3 + A_4) - A_9A_{10} - A_5A_8a_2^*\\ &\quad + A_7(A_5a_1^* + A_2A_3 + A_2A_4) +\\ &A_2A_7b^2 + (b^2a_1^* - A_4A_8 + A_3a_1 + A_6a_1^*)C_5 - A_1A_4\\ &\quad - A_1A_6 - A_1A_3)\alpha_1 - A_1A_4A_6 -\\ &A_3A_5A_8 - A_1A_5A_8 - A_6A_9A_{10}a_2^* - A_4A_9A_{10}\\ &\quad + A_7(A_2A_3A_4 + A_3A_5a_1^*) - a_2^*A_1A_3A_6 -\\ &A_3A_4A_6 + A_7(A_2A_3 + A_2A_4 + A_5a_1^*)b^2 + (-A_2A_8\\ &\quad + (A_3 + A_6)a_1^*)b^2)C_5 - A_1A_3A_4 \end{aligned}\right\},$$

$$B_4 = \left\{\begin{aligned} &((((-A_3 - A_6)b^2 - A_3A_6)\alpha_1 + (-A_3A_6 + \varepsilon_4\varepsilon_5)b^2\\ &\quad + A_3\varepsilon_4\varepsilon_5)C_5 + (-b^2A_5A_7 - A_3A_5A_7)\alpha_1 -\\ &A_3A_5A_7b^2)a_1^* + ((b^2A_2A_8 + A_2A_3AA_8)\alpha_1\\ &\quad + (A_2A_3A_8 - A_8\varepsilon_4)b^2 - A_3A_8\varepsilon_4)C_5 +\\ &((-A_2A_3A_7 - A_2A_4A_7)b^2 + A_1A_3A_6 + A_1A_4A_6\\ &\quad + A_1A_5A_8 + A_3(A_1A_4 + A_5A_8) + A_4A_9A_{10}\\ &+(A_3A_4 + A_9A_{10})A_6 - A_2A_3A_4A_7)\alpha_1\\ &\quad + (-A_2A_3A_4A_7 + (A_3A_7 + A_4A_7)\varepsilon_4)b^2\\ &\quad + A_1A_3(A_4A_6 +\\ &A_5A_8) + (A_4A_6A_9 + A_5A_8A_9)A_{10} + (A_3A_4A_7a_2^*\\ &\quad + (-A_1A_3 - A_1A_4 - A_3A_4 - A_9A_{10})\varepsilon_5)\varepsilon_4 \end{aligned}\right\},$$

$$B_5 = -\left\{\begin{aligned} &((A_3A_5A_7 + A_3A_6C_5)b^2\alpha_1 - b^2A_3C_5\varepsilon_5\varepsilon_4)a_1^*\\ &\quad + ((A_2A_3A_4A_7 - A_2A_3A_8C_5)b^2 -\\ &A_1A_3(A_4A_6 + A_5A_8) - (A_4A_6 + a_2^*A_5A_8)A_9A_{10})\alpha_1\\ &\quad + (A_4(A_1A_3 + A_9A_{10})\varepsilon_5 +\\ &(-A_3A_4A_7 + A_3A_8C_5)b^2)\varepsilon_4 \end{aligned}\right\}.$$

To facilitate the process, it is advantageous to simplify Eq. (37) with the roots: k_n^2 (n =1, 2, 3, 4, 5 : Re(k_n)> 0) by

$$(D^2 - k_1^2)(D^2 - k_2^2)(D^2 - k_3^2)(D^2 - k_4^2)(D^2 - k_5^2)\{\bar{\Theta}, \bar{N}, \bar{\Pi}, \bar{\varphi}, \bar{\psi}\}(x) = 0. \quad (38)$$

The solution expressed in linear form for Eq. (37) is as follows:

$$[\bar{\Theta}, \bar{\varphi}, \bar{\Pi}, \bar{N}, \bar{\psi}](x) = \sum_{i=1}^{5}[1, h_{1i}, h_{2i}, h_{3i}, h_{4i}]\mathrm{Q}_i(b, \omega)e^{-k_ix}. \quad (39)$$

The unknown quantities Q_i can be formulated when the other parameters are in the following form:

$$h_{1i} = \frac{((A_2C_5+A_5)k_i^6 + c_8k_i^4 + c_9k_i^2 + c_{10})}{(k_i^8 + c_4k_i^6 + c_5k_i^4 + c_6k_i^2 + c_7)},$$

$$h_{2i} = \frac{(A_2k_i^6 + c_1k_i^4 + c_2k_i^2 + c_3)}{(k_i^8 + c_4k_i^6 + c_5k_i^4 + c_6k_i^2 + c_7)},$$

$$h_{3i} = -\frac{(\varepsilon_4)}{(k_i^2 - \varepsilon_4)}, h_{4i} = \frac{(A_2A_{10}k_i^4 + c_{11}k_i^2 + c_{12})}{(k_i^8 + c_4k_i^6 + c_5k_i^4 + c_6k_i^2 + c_7)},$$

$$c_1 = (-A_2A_3 - A_2A_4 - A_2\alpha_1 - A_5a_1 + \varepsilon_4),$$

$$c_2 = (A_2A_3A_4 + A_2A_3\alpha_1 + A_2A_4\alpha_1 + A_3A_5a_1 + A_5a_1\alpha_1 - A_3\varepsilon_4 - A_4\varepsilon_4),$$

$$c_3 = -A_2A_3A_4\alpha_1 - A_3A_5a_1\alpha_1 + A_3A_4\varepsilon_4,$$

$$c_4 = C_5a_1 - A_1 - A_3 - A_4 - \alpha_1,$$

$$c_5 = -b^2C_5a_1 - A_3C_5a_1 - C_5a_1\alpha_1 + A_1A_3 + A_1A_4 + A_1\alpha_1 + A_3A_4 + A_3\alpha_1 + A_4\alpha_1 + A_9A_{10},$$

$$c_6 = b^2AC_5a_1 + b^2C_5a_1\alpha_1 + A_3C_5a_1\alpha_1 - A_1A_3A_4 - A_1A_3\alpha_1 - A_1A_4\alpha_1 - A_3A_4\alpha_1 - A_4A_9A_{10} - A_9A_{10}\alpha_1,$$

$$c_7 = -b^2A_3C_5a_1\alpha_1 + A_1A_3A_4\alpha_1 + A_4A_9A_{10}\alpha_1,$$

$$c_8 = -b^2A_2C_5 - A_2A_3C_5 - A_2C_5\alpha_1 - A_1A_5 - A_3A_5 - A_5\alpha_1 + C_5\varepsilon_4,$$

$$c_9 = b^2A_2A_3C_5 + b^2A_2C_5\alpha_1 - b^2C_5\varepsilon_4 + A_2A_3C_5\alpha_1 + A_1A_3A_5 + A_1A_5\alpha_1 + A_3A_5\alpha_1 - A_3C_5\varepsilon_4 + A_5AA_9A_{10},$$

$$c_{10} = -b^2A_2A_3C_5\alpha_1 + b^2A_3C_5\varepsilon_4 - A_1A_3A_5\alpha_1 - A_5A_9A_{10}\alpha_1,$$

$$c_{11} = A_{10}(-A_2A_4 - A_2\alpha_1 - A_5a_1 + \varepsilon_4),$$

$$c_{12} = A_{10}(A_2A_4\alpha_1 + A_5a_1\alpha_1 - A_4\varepsilon_4).$$

The components of displacement can be reformulated:

$$\begin{aligned} \bar{u}(x) &= -\sum_{n=1}^{5} \mathbb{Q}_n(k_nh_{2n} + ibh_{4n})e^{-k_nx}, \\ \bar{w}(x) &= \sum_{n=1}^{5} \mathbb{Q}_n(ibh_{2n} - k_nh_{4n})e^{-k_nx}. \end{aligned} \tag{40}$$

It is possible to write the constitutive Eq. (35) as:

$$\left.\begin{aligned} &\bar{\sigma}_{xx} \\ &= \sum_{n=1}^{5} \mathbb{Q}_n \frac{(h_{2n}(k_n^2 - b^2a_2) - A_2 - h_{3n} + a_1h_{1n} - ibk_nh_{4n}(a_2 - 1))}{1 - \xi^2(k_n^2 - b^2)} \\ &e^{-k_nx}, \\ &\bar{\sigma}_{zz} \\ &= \sum_{n=1}^{5} \mathbb{Q}_n \frac{(h_{2n}(a_2k_n^2 - b^2) - A_2 - h_{3n} + a_1h_{1n} - ibk_nh_{4n}(1 - a_2))}{1 - \xi^2(k_n^2 - b^2)} \\ &e^{-k_nx}, \\ &\bar{\sigma}_{xz} = -\sum_{n=1}^{5} a_4\mathbb{Q}_n \frac{ib(k_nh_{2n} + ibh_{4n}) + k_n(ibh_{2n} - k_nh_{4n})}{1 - \xi^2(k_n^2 - b^2)} e^{-k_nx}. \end{aligned}\right\} \tag{41}$$

4 Applications

When applying specific boundary restrictions to the free non-local microelongated surface, it is possible to evaluate arbitrary parameters. Choose your boundary conditions at [46], and then implement them in one of the following ways:

Mechanical boundary conditions can be selected, which can be represented by the normal stress on the non-local surface $x = 0$ as [43]:

$$\sigma_{xx}(0, z, t) = -\Upsilon, \tag{42}$$

where Υ is the load force falling on the surface.

For the tangential stress at $x = 0$, the other mechanical condition can be picked at will as:

$$\sigma_{xz} = 0 \Rightarrow \bar{\sigma}_{xz} = 0. \tag{43}$$

Because the temperature changes so rapidly (or at least in a short amount of time) in response to pulsed laser stimulation, relatively little heat is lost to the environment. Therefore, pulsed laser excitation is useful for absorption studies. Some energy-dependent physical reactions are also possible when a laser beam shines on a solid surface. A portion of the laser's energy is converted to heat when it strikes a material. When this happens, heat waves travel through the material and have their unique consequences. Consideration is also given to the fact that laser pulses are incident upon the medium's surrounding plane ($x = 0$). The following temperature scenario is applicable here [44]:

$$\Theta(x, z, t)|_{x=0} = L(z, t) = I\Phi(1 - R)h(z)g(t), \tag{44}$$

$$\begin{aligned} h(z) &= \frac{2}{\sqrt{2\pi}R^{\mathrm{G}}} \exp(-2z^2/R^{\mathrm{G}}), \\ g(t) &= \frac{8t^3}{V^2} \exp(-2t^2/V^2), \end{aligned} \tag{45}$$

where I represents the laser pulse energy per unit length, R expresses the surface reflectivity, Φ is the extinction coefficient, R^{G} denotes the radius of the Gaussian laser beam, and V represents the rise-time of the laser pulse.

An expression for the elongation condition of the scalar function could be:

$$\bar{\varphi} = 0. \tag{46}$$

After some time, the carriers will disperse close enough to the surface of the sample to be subject to recombination. This allows us to formulate the following expression for the carrier density boundary condition [47]:

$$\frac{\mathrm{d}\bar{N}}{\mathrm{d}x} = -\frac{\tilde{s}n_0}{D_E}, \tag{47}$$

where $\tilde{s}$ is the recombination speed of the carrier charge. Using the values of $\bar{\Theta}$, $\bar{\sigma}_{xx}$, $\bar{\sigma}_{xz}$, $\bar{\varphi}$, and $\bar{N}$, yields:

$$\left.\begin{aligned}
&\sum_{n=1}^{5}\mathbb{Q}_n\frac{(h_{2n}(k_n^2-b^2a_2)-A_2-h_{3n}+a_1h_{1n}-ibk_nh_{4n}(a_2-1))}{1-\xi^2(k_n^2-b^2)}\\
&\quad=\bar{\Upsilon}(s),\\
&\sum_{n=1}^{5}ib\mathbb{Q}k_n(h_{2i}-1)+(1+k_5^2)\Lambda_5=0,\\
&\sum_{n=1}^{5}-k_n\mathbb{Q}_n(b,\omega)=\bar{L}(z,t),\\
&\sum_{n=1}^{5}h_{1n}\mathbb{Q}_n(b,\omega)=0,\\
&\sum_{n=1}^{5}h_{3n}k_n\mathbb{Q}_n(b,\omega)=\frac{\tilde{s}\tilde{n}_0}{D_E}.
\end{aligned}\right\}. \quad (48)$$

5 Particular cases

1) The non-local magneto-thermoelasticity theory of rotating microelongation is derived by taking into account the modification of thermal conductivity and ignoring the effect of photo-electronic plasma (*i.e.*, $N = 0$) [14,15].
2) When the elongation parameters α_0, λ_0, and λ_1, are disregarded, the action of the magneto-photo-electronics plasma impact yields the rotational non-local photo-thermoelasticity theory with the variable thermal conductivity.
3) When the non-local component (*i.e.* $\xi = 0$). is removed, models of rotating magneto-photo-thermoelasticity are derived, which include elongation and temperature-dependent thermal conductivity.
4) When the angular velocity is ignored, the non-local magneto-photo-thermoelasticity theory predicted by the variable thermal conductivity is confirmed by observations of elongation (*i.e.* $\Omega = 0$) [20,22].
5) In the presence of the parameter H_0, in this case, the problem is studied with the effect of a magnetic field and the rotational non-local photo-thermoelasticity model appears under the effect of a laser pulse.
6) When the thermal conductivity of the medium does not vary on temperature, the elongation rotational non-local magneto-photo-thermoelasticity model is obtained (*i.e.* $\pi = 0$, and hence, $K = K_0$).

Maps can be used to represent temperatures before conversion, and the relationship between and the maps' transform is represented by Eqs. (8) and (9) as:

$$\Theta = \frac{1}{K_0}\int_0^T K_0(1+\pi T)\mathrm{d}T = T+\frac{\pi}{2}T^2 = \frac{\pi}{2}\left(T+\frac{1}{\pi}\right)^2-\frac{1}{2\pi}, \quad (49)$$

or

$$T = \frac{1}{\pi}[\sqrt{1+2\pi\Theta}-1] = \frac{1}{\pi}[\sqrt{1+2\pi\bar{\Theta}e^{\omega t+ibz}}-1]. \quad (50)$$

6 Discussions of the numerical results

To gain a deeper understanding of the issue and to shed light on how relaxation durations, rotation, non-local parameters, and thermal conductivity influence the physical field variables under the propagating waves, a numerical analysis is performed with the help of MATLAB (2022a) software. For our numerical calculations, we have settled on a polymer silicon (Si, n-type) semiconductor material. The physical constants of Si media, shown above, are expressed in SI units [30,31]:

$\lambda = 3.64 \times 10^{10}$ N/m^2, $\mu = 5.46 \times 10^{10}$ N/m^2, $\rho = 2,330$ kg/m^3, $T_0 = 800$ K, $\tau = 5 \times 10^{-5}$ s, $d_n = -9 \times 10^{-31}$ m^3, $D_\mathrm{E} = 2.5 \times 10^{-3}$ m^2/s, E_g =1.11 eV, $\tilde{s} = 2$ m/s, $C_\mathrm{E} = 695$ J/(kg K), $\alpha_{t_1} = 0.04 \times 10^{-3}$ K^{-1}, $\alpha_{t_2} = 0.017\mathrm{x}\,10^{-3}$ K^{-1}, $K = 150$ Wm^{-1} K^{-1}, $\lambda_0 = 0.5 \times 10^{10}$ Nm^{-2}, $t = 0.001$,

$j = 0.2 \times 10^{-19}$ m^2, $\gamma = 0.779 \times 10^{-9}$ N, $k = 10^{10}$ Nm^{-2}, $\tilde{n}_0 = 10^{20}$ m^{-3}, $\lambda_1 = 0.5 \times 10^{10}$ Nm^{-2}, $\alpha_0 = 0.779 \times 10^{-9}$ N, $\tau_0 = 0.00005$, $\nu_0 = 0.0005$, $R^\mathrm{G} = 0.45$ mm, $V = 10$ ns, $\Phi = 0.001$ m^{-1}, $I = 10$J, $\mu_0 = 4\pi \times 10^{-7}$ H/m.

To acquire wave propagations of the relevant physical variables in 2D according to a tiny value of time, numerical computations are performed here using the dimensionless fields. Numerical calculations necessitate the inclusion of extra problem constants such as $z = -1$, $b = 1$, $\bar{L} = 1$, ζ= 0.05, $\bar{\Upsilon} = 2$, and $\omega_0 = -2.5$ in the range $0 \le x \le 5$.

6.1 Impact of variable thermal conductivity parameter

Figure 2 (composed of six subfigures) depicts the influence of various non-positive parameters π on the wave propagation of the main physical field distributions *vs* the horizontal distance for the range of $0 \le x \le 10$. This diagram compares three different scenarios. The first is met when the medium is temperature independent, denoted when $\pi = 0(K = K_0)$ [61]. When $\pi = -0.3$ and $\pi = -0.6$, respectively, the second and third scenarios illustrate how the medium responds to a change in temperature. The GL model dictates a periodic propagation of thermal, non-local elongation, elastic, plasma, and mechanical waves when $t = 0.001$ and $\Omega = 0.5$ under the influence of laser pulses when $V = 1.2$ and magnetic fields according to the GL model. In the case of temperature, the thermal wave is initially positive at the free surface, before increasing in the initial range towards the edge and eventually reaching its maximum value as a result of the thermal loads

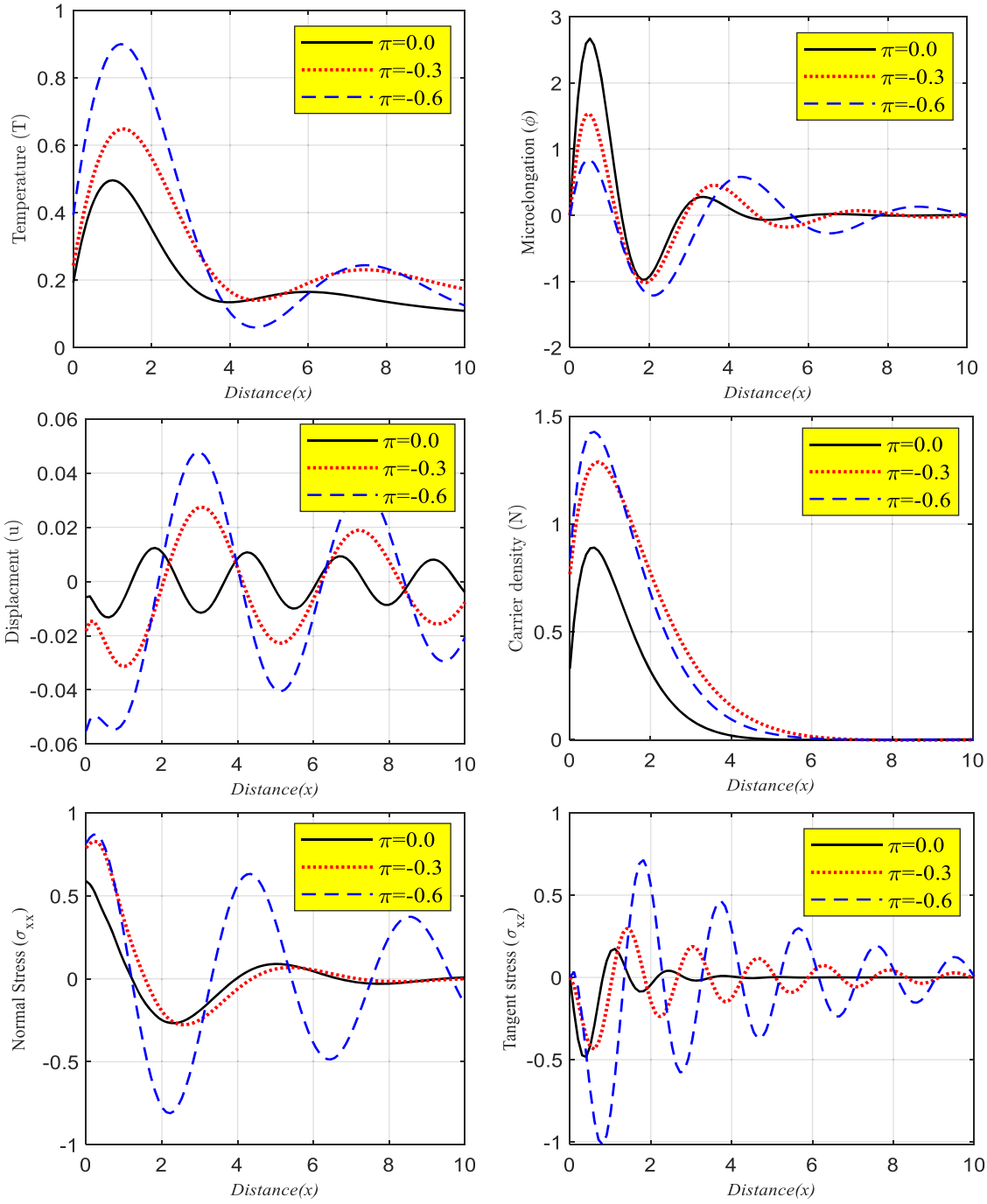

Figure 2: Variation of main quantities *versus* horizontal distance and different values of variable thermal conductivity when the laser pulse rise-time V = 1.2 under the impact of magnetic field according to the GL model for rotational non-local medium.

introduced by the laser beams and mechanical load. As a result, the thermal wave steadies when it reaches the minimum value in the second range and aligns with the zero line. As the parameter is raised, a large increase is observed in the magnitude of the temperature distribution. Plasma waves, which have a carrier density with an optoelectronic distribution, share the same properties as thermal waves. In contrast, increasing the parameter reduces the magnitude of the dispersion of plasma waves, which agrees with experimental results [62]. The second inset shows that for all three values of the parameter π, the microelongation distribution begins at zero at the boundary. Microelongation function obtains its maximum value early on, close to the non-local surface, and then its magnitude of profile begins to

diminish with increasing distance, as seen in the inset figure. As distance is increased, the elastic wave (displacement) solution curves begin in each case with a different initial magnitude. Normal displacement is highly sensitive to the variable thermal conductivity parameter, as seen by a decrease in numerical values as the parameter's value is increased. The normal stress fluctuations with distance are depicted in the fifth inset for all three cases ($\pi = 0$, $\pi = -0.3$, and $\pi = -0.6$). The mechanical loaded boundary conditions of the problem are accounted for by the fact that the normal stress magnitudes start positive, increase to their maximums, then decrease and increase again to their zero-point values. In all cases, normal stress values are greatest close to the source and decrease steadily to zero thereafter. The sixth subfigure uses three different values of variable thermal conductivity ($\pi = 0$, $\pi = -0.3$ and $\pi = -0.6$) to show

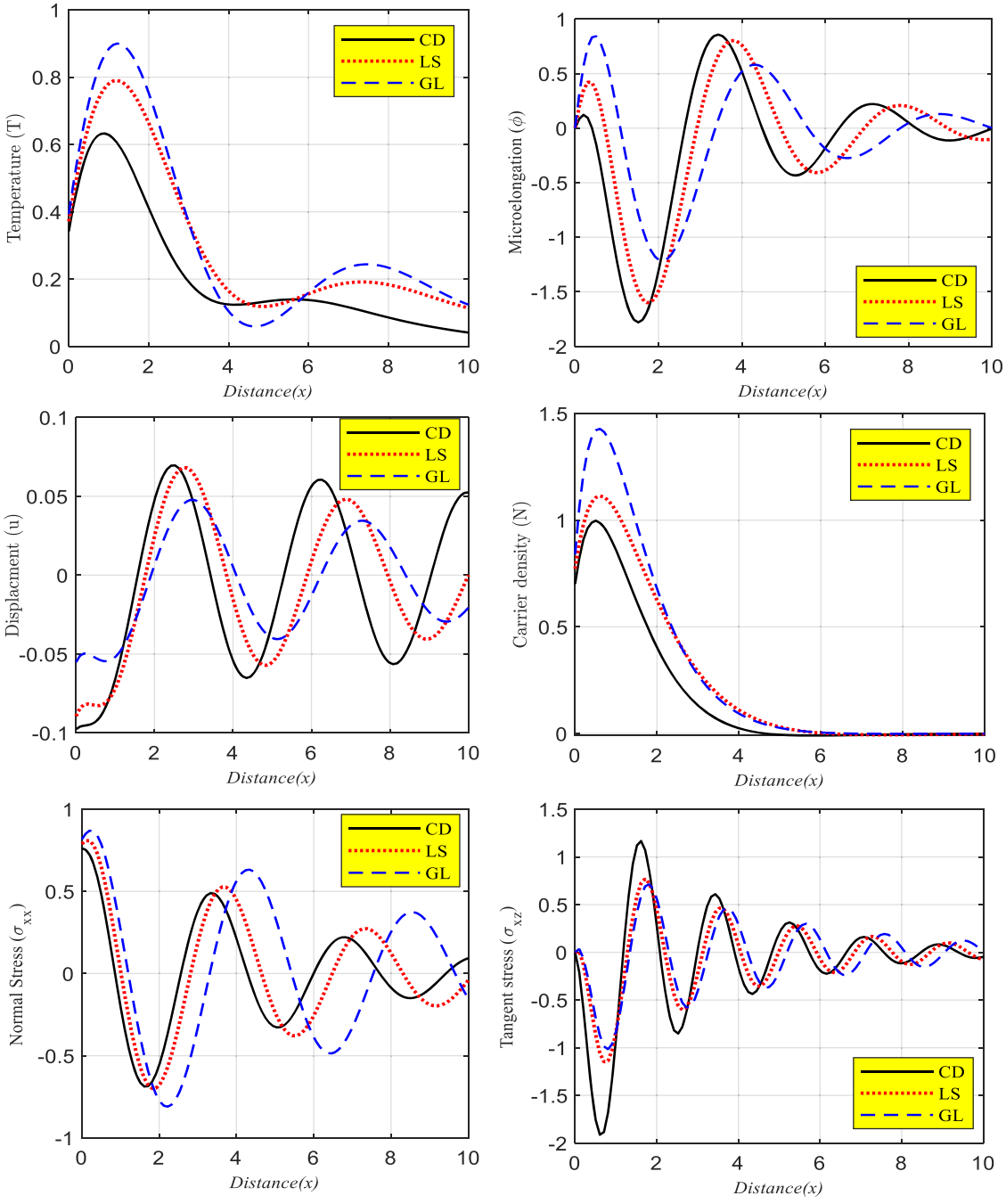

Figure 3: Variation of main quantities *versus* horizontal distance of different values of photo-thermoelasticity models under the effect of magnetic field and laser pulse rise-time $V = 1.2$ when $\pi = 0.6$ for rotational non-local medium.

how the tangential stress varies with the distance. The non-local boundary condition ensures that the tangential stress always begins at zero magnitude. In the inset, we can see that as the values of the variable thermal conductivity are increased, the tangential stress also rises numerically.

6.2 Photo-thermoelasticity models

The variations of the fundamental physical variables are shown with distance in Figure 3, and the numerical calculations are carried out under the influence of laser pulses

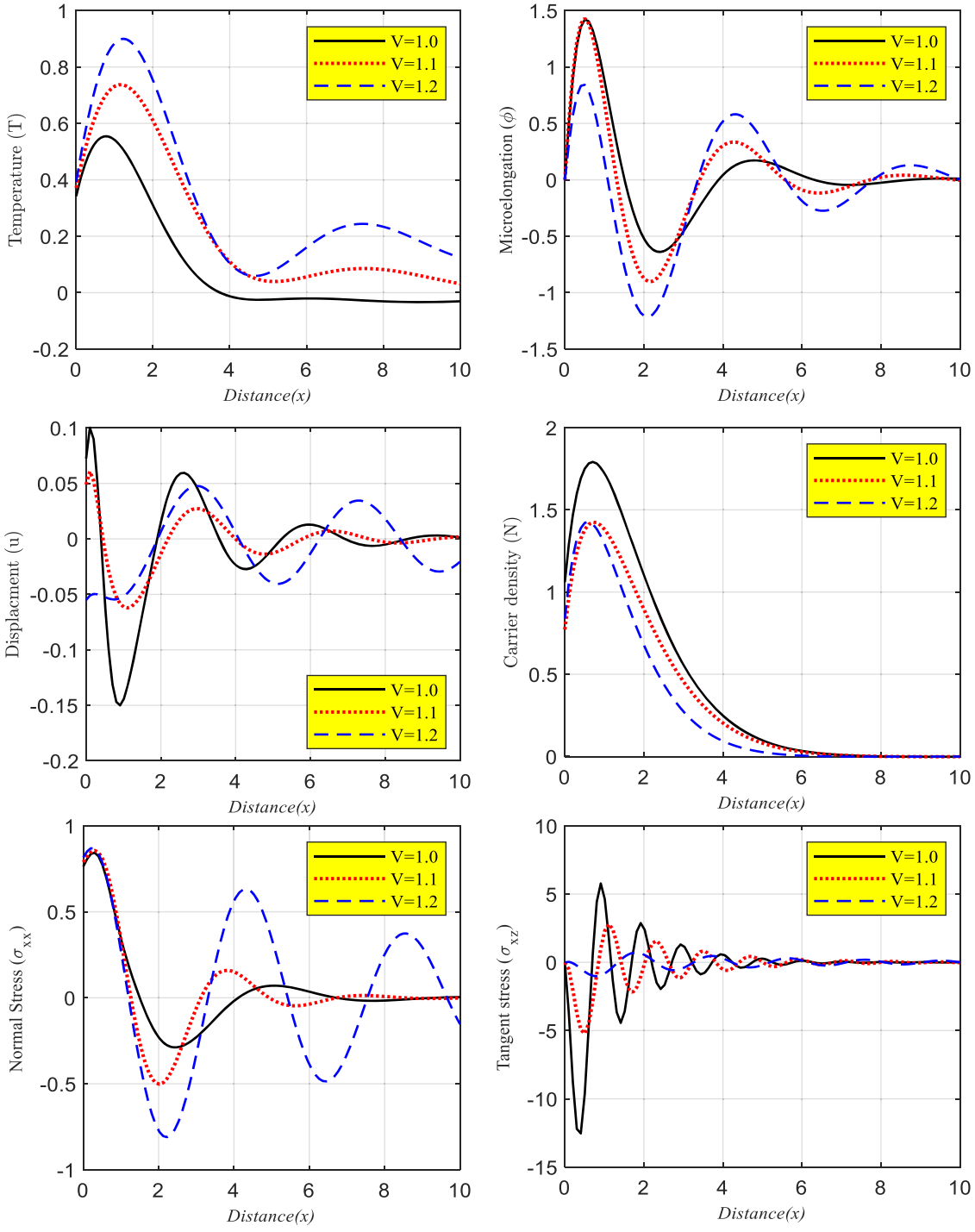

Figure 4: Variation of main quantities *versus* horizontal distance and different values of the laser pulse rise-time V when $\pi = 0.6$ under the impact of magnetic field according to the GL model for rotational non-local medium.

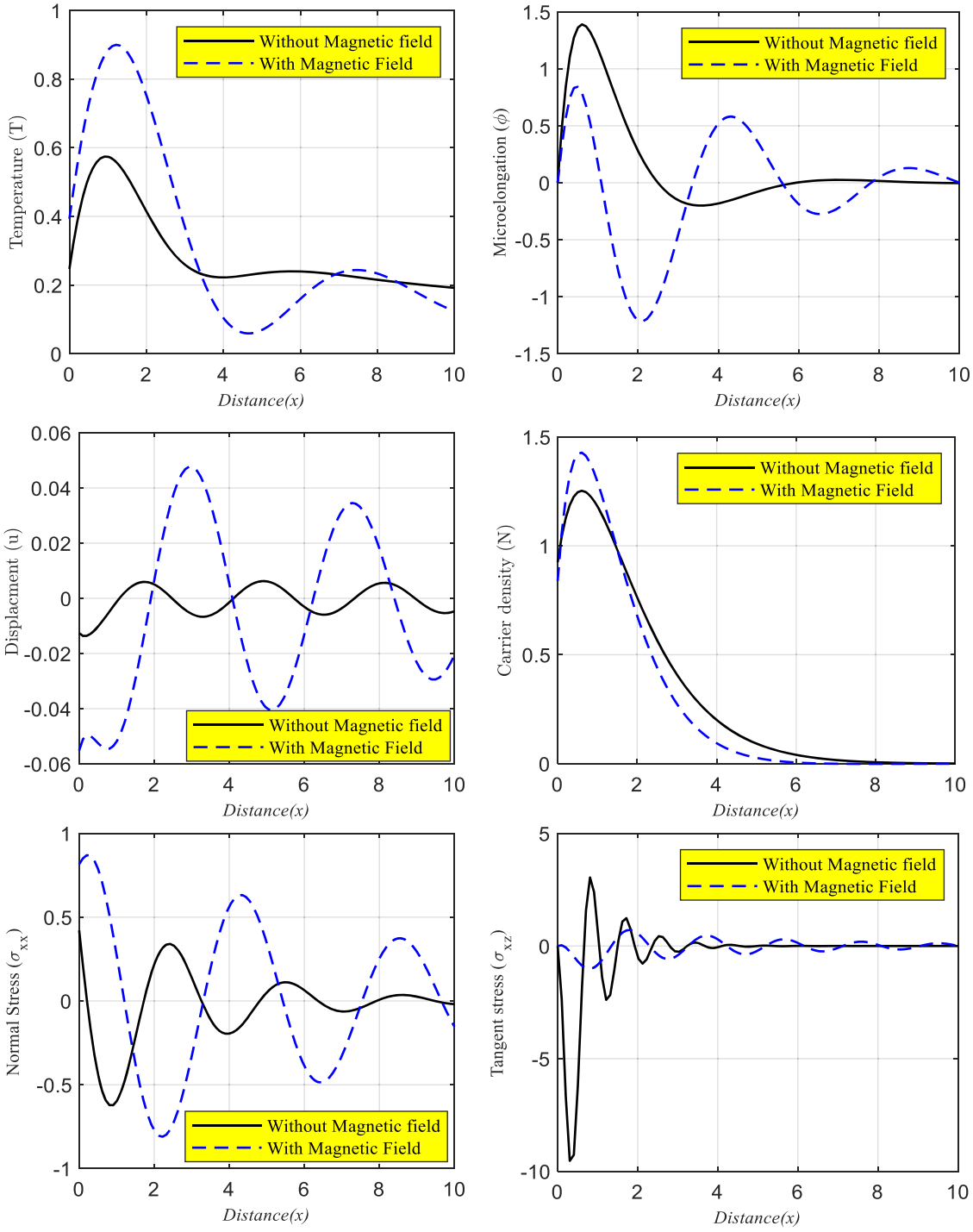

Figure 5: Variation of main quantities *versus* horizontal distance in the absence and presence of magnetic field under the effect of laser pulse rise-time $V = 1.2$ when $\pi = 0.6$ according to the GL model for rotational non-local medium.

and magnetic field. These fluctuations are displayed for three distinct values of the relaxation times according to the photo-thermoelasticity models. The non-local boundary condition is satisfied for the rotation ($\Omega = 0.5$) when the elongation-nonlocality qualities exhibit the same pattern of variations when the solution curves for the three different relaxation time values originate from the surface ($0 \le x \le 10$) when $\pi = -0.6$. In Figure 3, all of the solution curves coincide with a line with zero magnitudes, even though the distances between the three values

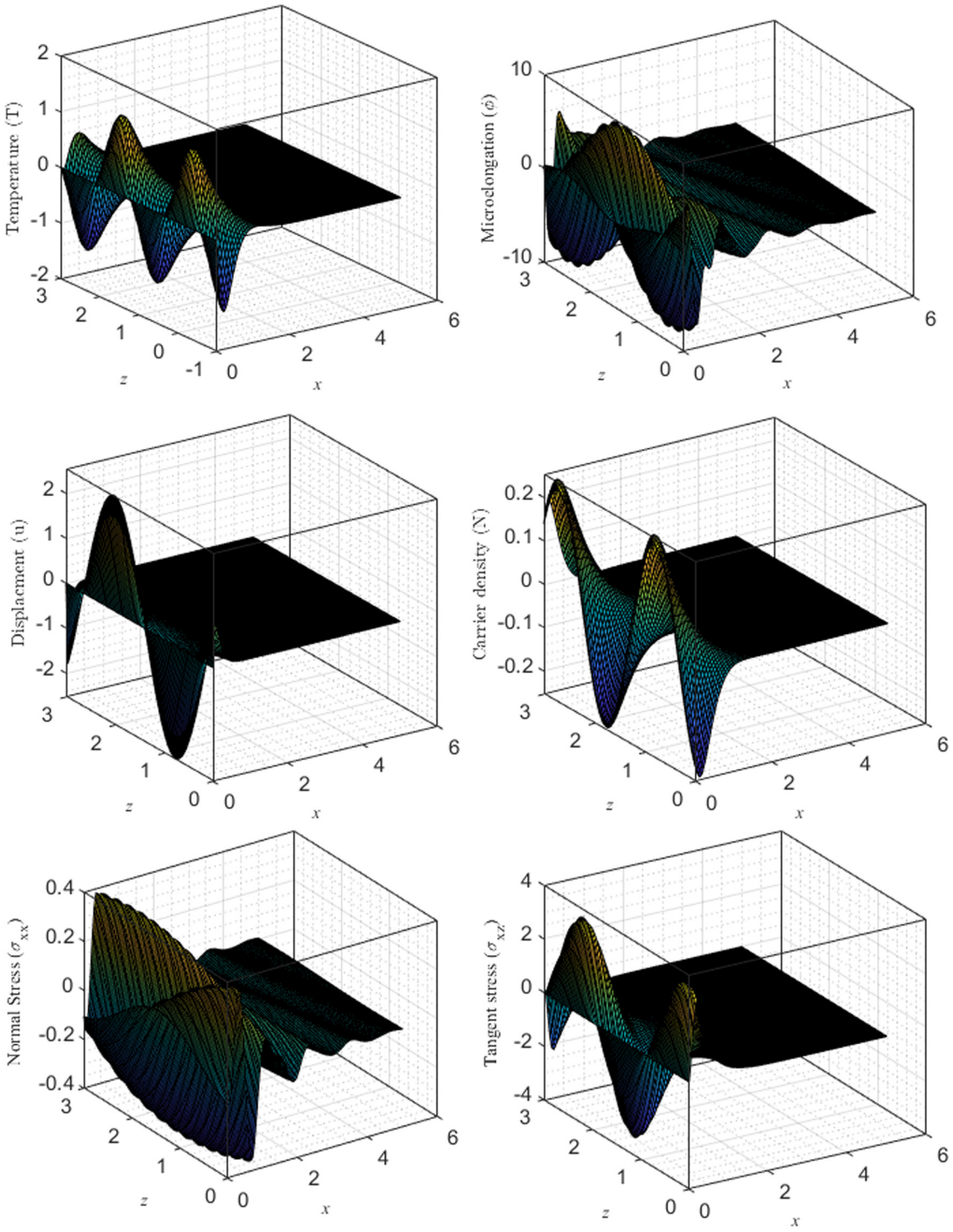

Figure 6: Changes in the fundamental physical fields as a function of horizontal and vertical distances, as well as changing thermal conductivity according to the DPL model under the effect of magnetic field and laser pulse.

and the equilibrium state are getting further apart. It should come as no surprise that the relaxation times have a significant impact on the dispersion of the waves that were studied.

6.3 Impact of the laser pulse rise-time

The maximal laser energy density at the silicon surface is related not only to the pulse energy and the spot size of the

picosecond laser pulses but also to the rise-time of these pulses. The third group (Figure 4) displays, under the influence of a magnetic field, the influence of the laser pulse rise-time parameter V on the investigated system variables *versus* location when $\Omega = 0.5$ under the effect magnetic field according to the GL model for three different values of V equal to 0.1, 0.2, and 0.3. As can be seen in the inset subfigures, the boundary conditions for all physical quantities are satisfied, and all curves coincide as x tends to infinity. We discover that the rise-time parameter V of the laser pulse has a significant effect (PT influence) for distances x between 0 and 10. The greatest temperature of the structure is consistently found in the front of the heat wave, and it decreases progressively with increasing depth within the medium, as shown by the numerical data. An unusual mechanical force is generated by the femtosecond laser. High-quality surfaces can be made with femtosecond lasers with minimal collateral damage compared to other methods, such as continuous or long-pulse laser heat generation. This is because of the mechanisms behind the generation of mechanical forces and the rapid deformation of lattices. The ultrafast PT response over a range of around three orders of magnitude can be explained by the PT mechanical model, which accounts for all of these effects starting in the femtosecond timescale, where electron-to-phonon interactions predominate. Furthermore, it can account for such behavior on timescales of tens of picoseconds, where phonon-to-phonon interactions predominate.

6.4 Impact of the magnetic field

Figure 5 is a scatter plot used to analyze the effect of the magnetic field on all of the distributions in the medium. Within the entire study region, we compare two examples (without and with magnetic field) at the small-time scale according to the GL theory for rotational media when under the action of the laser pulse. Figure 5 (which consists of six subfigures) depicts qualitative behavior that has been demonstrated. Figure 5 shows that the action of the magnetic field leads to an increase in all the field variables measured. Those two areas are the optoelectronics subfield and the elongation function. There is a greater impact of the external magnetic field on all distributions.

6.5 The 3D representation

The changes in the nonlocality of fundamental physical fields as a function of horizontal and vertical distance are depicted in a three-dimensional plot shown in Figure 6. These simulations were performed to investigate the effect of magnetic field and laser pulse on the interaction between mechanical–plasm–elastic waves in silicon according to the GL model under the effect of rotation. All of these distributions tend to shrink as the time and space window widens, eventually settling into a new equilibrium. Elastic–thermal plasma and mechanical waves are particularly sensitive to the magnetic field and laser pulse effect on the interaction between electron and hole charge carrier fields in the initial region near the boundary.

7 Conclusion

Two-dimensional deformation of a homogeneous, isotropic, microelongated semiconducting half-space is the primary focus of the mentioned research, which is conducted within the context of photo-thermoelasticity. The models in this work allow for a range of thermal conductivities, and the authors hope to learn more about how changing this parameter, along with thermal relaxation times, time rise of laser pulse and magnetic field, affects other physical quantities. A thermoelastic model was employed to make these predictions because of the laser source's finite width and lifetime. The laser pulse was employed to heat the semiconductor material, and its time-dependent behavior concerning its long-range thermoelastic characteristics was studied. The results indicate that the thermal conductivity parameter has a significant impact on the wave propagation behavior of the physical quantities over a broad range. Variations in the thermal relaxation time are found to increase the magnitudes of the principal physical fields. In addition, there is a natural tendency for all waves traveling within the fundamental fields to balance out. The distribution of physical quantities within a nonlocality medium is profoundly affected by the existence of a magnetic field in the microelongated semiconductor medium, together with different values of relaxation time. It is also discovered that the analyzed physical variables wave propagation is significantly affected by the time rias of laser pulse parameter. It was determined that the laser pulse's rising time is a significant factor that meaningfully influences all other fields. Microelongated semiconductor silicon is worth investigating further because of its potential applications in modern electronic devices like smartphones, sensors, computer processors, medical equipment, diodes, accelerometers, inertial sensors, and electric circuits.

Acknowledgments: The authors extend their appreciation to Princess Nourah bint Abdulrahman University for funding this research under Researchers Supporting Project

number (PNURSP2023R154) Princess Nourah bint Abdulrahman University, Riyadh, Saudi Arabia.

Funding information: The authors extend their appreciation to Princess Nourah bint Abdulrahman University for funding this research under Researchers Supporting Project number (PNURSP2023R154), Princess Nourah bint Abdulrahman University, Riyadh, Saudi Arabia.

Author contributions: All authors have accepted responsibility for the entire content of this manuscript and approved its submission.

Conflict of interest: The authors state no conflict of interest.

Data availability statement: The datasets generated and/or analysed during the current study are available from the corresponding author on reasonable request.

References

[1] Eringen AC. Microcontinuum field theories. Foundations and Solids. Vol. 1. New York: Springer Verlag; 1999.
[2] Eringen AC. Linear theory of micropolar elasticity. J Math Mech. 1966;15(6):909–23.
[3] Eringen AC. Theory of thermo-microstretch elastic solids. Int J Eng Sci. 1990;28(12):1291–301.
[4] Singh B. Reflection and refraction of plane waves at a liquid/thermo-microstretch elastic solid interface. Int J Eng Sci. 2001;39(5):583–98.
[5] Othman M, Lotfy K. The influence of gravity on 2-D problem of two temperature generalized thermoelastic medium with thermal relaxation. J Comput Theor Nanosci. 2015;12:2587–600.
[6] De Cicco, Nappa L. On the theory of thermomicrostretch elastic solids. J Therm Stress. 1999;22(6):565–80.
[7] Abouelregal A, Marin M. The response of nanobeams with temperature-dependent properties using state-space method via modified couple stress theory. Symmetry. 2020;12(8):Art. No. 1276.
[8] Marin M, Ellahi R, Vlase S, Bhatti M. On the decay of exponential type for the solutions in a dipolar elastic body. J Taibah Univ Sci. 2020;14(1):534–40.
[9] Marin M, Chirila A, Othman M. An extension of Dafermos's results for bodies with a dipolar structure. Appl Math Comput. 2019;361:680–8.
[10] Ramesh G, Prasannakumara B, Gireesha B, Rashidi M. Casson fluid flow near the stagnation point over a stretching sheet with variable thickness and radiation. J Appl Fluid Mech. 2016;9(3):1115–22.
[11] Ezzat M, Abd-Elaal M. Free convection effects on a viscoelastic boundary layer flow with one relaxation time through a porous medium. J Frankl Inst. 1997;334(4):685–706.
[12] Shaw S, Mukhopadhyay B. Periodically varying heat source response in a functionally graded microelongated medium. Appl Math Comput. 2012;218(11):6304–13.
[13] Shaw S, Mukhopadhyay B. Moving heat source response in a thermoelastic micro-elongated Solid. J Eng Phys Thermophys. 2013;86(3):716–22.
[14] Ailawalia P, Sachdeva S, Pathania D. Plane strain deformation in a thermo-elastic microelongated solid with internal heat source. Int J Appl Mech Eng. 2015;20(4):717–31.
[15] Sachdeva S, Ailawalia P. Plane strain deformation in thermoelastic micro-elongated solid, Civil. Env Res. 2015;7(2):92–8.
[16] Ailawalia P, Kumar S, Pathania D. Internal heat source in thermo-elastic micro-elongated solid under Green Lindsay theory. J Theor Appl Mech. 2016;46(2):65–82.
[17] Marin M, Vlase S, Paun M. Considerations on double porosity structure for micropolar bodies. AIP Adv. 2015;5(3):037113.
[18] Gordon JP, Leite RCC, Moore RS, Porto SPS, Whinnery JR. Long-transient effects in lasers with inserted liquid samples. Bull Am Phys Soc. 1964;119:501–10.
[19] Kreuzer LB. Ultralow gas concentration infrared absorption spectroscopy. J Appl Phys. 1971;42:2934.
[20] Tam AC. Ultrasensitive laser spectroscopy. New York: Academic Press; 1983. p. 1–108.
[21] Tam AC. Applications of photoacoustic sensing techniques. Rev Mod Phys. 1986;58:381.
[22] Tam AC. Photothermal investigations in solids and fluids. Boston: Academic Press; 1989. p. 1–33.
[23] Hobinya A, Abbas I. A GN model on photothermal interactions in a two-dimensions semiconductor half space. Results Phys. 2019;15:102588.
[24] Todorovic DM, Nikolic PM, Bojicic AI. Photoacoustic frequency transmission technique: electronic deformation mechanism in semiconductors. J Appl Phys. 1999;85:7716.
[25] Song YQ, Todorovic DM, Cretin B, Vairac P. Study on the generalized thermoelastic vibration of the optically excited semiconducting microcantilevers. Int J Solids Struct. 2010;47:1871.
[26] Lotfy K. A novel model of photothermal diffusion (PTD) fo polymer nano- composite semiconducting of thin circular plate. Phys B-Condenced Matter. 2018;537:320–8.
[27] Lotfy K. A novel model for Photothermal excitation of variable thermal conductivity semiconductor elastic medium subjected to mechanical ramp type with two-temperature theory and magnetic field. Sci Rep. 2019;9:ID 3319.
[28] Lotfy K. Effect of variable thermal conductivity during the photothermal diffusion process of semiconductor medium. Silicon. 2019;11:1863–73.
[29] Abbas I, Alzahranib F, Elaiwb A. A DPL model of photothermal interaction in a semiconductor material. Waves Random Complex Media. 2019;29:328–43.
[30] Mahdy A, Lotfy Kh, El-Bary A, Alshehri H, Alshehri A. Thermal-microstretch elastic semiconductor medium with rotation field during photothermal transport processes. Mech Based Des Struct Mach. 2023;51(6):3176–93. doi: 10.1080/15397734.2021.1919527.
[31] Lotfy K, El-Bary A. Magneto-photo-thermo-microstretch semiconductor elastic medium due to photothermal transport process. Silicon. 2022;14:4809–21. doi: 10.1007/s12633-021-01205-1.
[32] Eringen A, Edelen D. On nonlocal elastic. Int J Eng Sci. 1972;10:233–48.
[33] Eringen A. On differential equations of nonlocal elasticity and solutions of screw dislocation and surface waves. J Appl Phys. 1983;54:4703–10.
[34] Chteoui R, Lotfy Kh, El-Bary A, Allan M. Hall current effect of magnetic-optical elastic-thermal-diffusive non-local semiconductor model during electrons-holes excitation processes. Crystals. 2022;12:1680.
[35] Sheoran S, Chaudhary S, Deswal S. Thermo-mechanical interactions in a nonlocal transversely isotropic material with rotation under

Lord-Shulman model. Waves Random Complex Media. 2021. doi: 10.1080/17455030.2021.1986648.
[36] Sheoran S, Chaudhary S, Kalkal K. Nonlocal thermodynamical vibrations in a rotating magneto-thermoelastic medium based on modified Ohm's law with temperature-dependent properties. Multidiscip Model Mater Struct. 2022;18(6):1087–112. doi: 10.1108/MMMS-05-2022-0089.
[37] Chaudhary S, Kalkal K, Sheoran S. Photothermal interactions in a semiconducting fiber-reinforced elastic medium with temperature-dependent properties under dual-phase-lag model. ZAMM-J Appl Math Mech. 2023;103:e202300316. doi: 10.1002/zamm.202300316.
[38] Biswas S. Surface waves in porous nonlocal thermoelastic orthotropic medium. Acta Mech. 2020;231:2741–60. doi: 10.1007/s00707-020-02670-2.
[39] Biswas S. Rayleigh waves in a nonlocal thermoelastic layer lying over a nonlocal thermoelastic half-space. Acta Mech. 2020;231:4129–44. doi: 10.1007/s00707-020-02751-2.
[40] Biswas S. The propagation of plane waves in nonlocal visco-thermoelastic porous medium based on nonlocal strain gradient theory. Waves Random Complex Media. 2021. doi: 10.1080/17455030.2021.1909780.
[41] Tiwari R, Saeed R, Kumar A, Kumar A, Singhal A. Memory response on generalized thermoelastic medium in context of dual phase lag thermoelasticity with non-local effect. Arch Mech. 2022;74(2–3):69–88. doi: 10.24423/aom.3926.
[42] Tiwari R, Singhal A, Kumar A. Effects of variable thermal properties on thermoelastic waves induced by sinusoidal heat source in half space medium. Mater Today: Proc. 2022;62(8):5099–104. doi: 10.1016/j.matpr.2022.02.442.
[43] Kumar R, Tiwari R, Singhal A. Analysis of the photo-thermal excitation in a semiconducting medium under the purview of DPL theory involving non-local effect. Meccanica. 2022;57:2027–41. doi: 10.1007/s11012-022-01536-2.
[44] Singhal A, Sedighi H, Ebrahimi F, Kuznetsova I. Comparative study of the flexoelectricity effect with a highly/weakly interface in distinct piezoelectric materials (PZT-2, PZT-4, PZT-5H, LiNbO3, BaTiO3). Waves Random Complex Media. 2021;31(6):1780–98. doi: 10.1080/17455030.2019.1699676.
[45] Nirwal S, Sahu S, Singhal A, Baroi J. Analysis of different boundary types on wave velocity in bedded piezo-structure with flexoelectric effect. Compos Part B: Eng. 2019;167:434–47. doi: 10.1016/j.compositesb.2019.03.014.
[46] Sahu S, Singhal A, Chaudhary S. Surface wave propagation in functionally graded piezoelectric material: An analytical solution. J Intell Mater Syst Struct. 2018;29(3):423–37. doi: 10.1177/1045389X17708047.
[47] Kaur I, Singh K. Nonlocal memory dependent derivative analysis of a photo-thermoelastic semiconductor resonator. Mech Solids. 2023;58:529–53. doi: 10.3103/S0025654422601094.
[48] Kaur I, Singh K. Effect of memory dependent derivative and variable thermal conductivity in cantilever nano-Beam with forced transverse vibrations. Forces Mech. 2021;5:100043. doi: 10.1016/j.finmec.2021.100043.
[49] Kaur I, Singh K. Plane wave in non-local semiconducting rotating media with Hall effect and three-phase lag fractional order heat transfer. Int J Mech Mater Eng. 2021;16:14. doi: 10.1186/s40712-021-00137-3.
[50] Sarkar N, Mondal S, Othman M. L–S theory for the propagation of the photo-thermal waves in a semiconducting nonlocal elastic medium. Waves Random Complex Media. 2022;32(6):2622–35. doi: 10.1080/17455030.2020.1859161.
[51] Sarkar N. Thermoelastic responses of a nonlocal elastic rod due to nonlocal heat conduction. Z Angew Math Mech. 2020;100:e201900252. doi: 10.1002/zamm.201900252.
[52] Sharma D, Thakur P, Sarkar N, Bachher M. Vibrations of a nonlocal thermoelastic cylinder with void. Acta Mech. 2020;231:2931–45. doi: 10.1007/s00707-020-02681-z.
[53] Sharma D, Bachher M, Manna S, Sarkar N. Vibration analysis of functionally graded thermoelastic nonlocal sphere with dual-phase-lag effect. Acta Mech. 2020;231:1765–81. doi: 10.1007/s00707-020-02612-y.
[54] Yang L, Zhang B, Klemeš J, Liu J, Song M, Wang J. Effect of buried depth on thermal performance of a vertical U-tube underground heat exchanger. Open Phys. 2021;19(1):327–30. doi: 10.1515/phys-2021-0033.
[55] Trivedi N, Das S, Craciun EM. The mathematical study of an edge crack in two different specified models under time-harmonic wave disturbance. Mech Compos Mater. 2022;58:1–14. doi: 10.1007/s11029-022-10007-4.
[56] Cristescu N, Craciun EM, Soós E. Mechanics of elastic composites. USA: Chapman and Hall/CRC; 2004.
[57] Youssef H, El-Bary A. Two-temperature generalized thermoelasticity with variable thermal conductivity. J Therm Stresses. 2010;33:187–201.
[58] Lord H, Shulman Y. A generalized dynamical theory of thermoelasticity. J Mech Phys Solid. 1967;15:299–309.
[59] Green A, Lindsay K. Thermoelasticity. J Elast. 1972;2:1–7.
[60] Biot M. Thermoelasticity and irreversible thermodynamics. J Appl Phys. 1956;27:240–53.
[61] Mandelis A, Nestoros M, Christofides C. Thermoelectronic-wave coupling in laser photothermal theory of semiconductors at elevated temperatures. Opt Eng. 1997;36(2):459–68.
[62] Liu J, Han M, Wang R, Xu S, Wang X. Photothermal phenomenon: Extended ideas for thermophysical properties characterization. J Appl Phys. 2022;131:065107. doi: 10.1063/5.0082014.